

Isolation and Characterization of Heteroleptic Mononuclear Palladium(I) Complexes

Giang N. Tran,[†] Bailey S. Bouley,[†] and Liviu M. Mirica*



Cite This: *J. Am. Chem. Soc.* 2022, 144, 20008–20015



Read Online

ACCESS |



Metrics & More

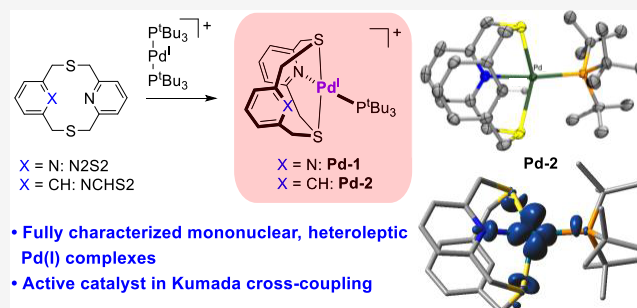


Article Recommendations



Supporting Information

ABSTRACT: Catalytic transformations involving Pd(0)/Pd(II) catalytic cycles are very well known, and processes involving high-valent Pd(III) and Pd(IV) and low-valent Pd(I) intermediates have also gained interest in recent years. Although low-valent Pd(I) intermediates are proposed in these catalytic cycles, isolated and characterized mononuclear Pd(I) species are very rare. Herein, we report the isolation of two heteroleptic mononuclear Pd(I) complexes stabilized by dithiapyridinophane ligands that were fully characterized by single-crystal X-ray diffraction; EPR, IR, UV–vis spectroscopies; and computational studies. Excitingly, one of these Pd(I) complexes shows Kumada Csp³–Csp² cross-coupling competency, and initial studies of the other shows direct evidence for Csp³–H bond activation proposed to occur at the Pd(I) center.



INTRODUCTION

Palladium-catalyzed organic transformations have gained tremendous interest over the past few decades, especially in the context of cross-coupling reactions.^{1–3} In these systems, while the general reaction mechanism involves a Pd⁰/Pd^{II} catalytic cycle, several reported catalytic systems proposed the involvement of Pd^I intermediates,^{4–10} in particular dinuclear Pd^I complexes that act as precatalysts for cross-coupling reactions.^{11–24} In addition, besides the other examples of dinuclear Pd^I complexes^{25–30} or transient mononuclear Pd^I species,^{31–38} there are very few examples of well-established mononuclear Pd complexes bearing a formal +1 oxidation state at Pd. To the best of our knowledge, only three structurally characterized examples of isolated Pd^I complexes have been reported: the cationic [Pd^I(P^tBu₃)₂]⁺ species and the [Pd^I(MeCN)(P^tBu₃)₂]⁺ complex, which were reported independently by Chaplin's and Ozerov's groups, respectively,^{39,40} and a recent heteroleptic, formally Pd^I complex supported by a redox noninnocent amide ligand.⁴¹ With the goal of isolating and characterizing mononuclear Pd^I species and exploring their reactivity, we report herein the synthesis and characterization of two unique heteroleptic mononuclear Pd^I complexes supported by dithiapyridinophane ligands. Importantly, one of these complexes exhibits catalytic reactivity in the Kumada cross-coupling reaction that is superior to its Pd⁰ or Pd^{II} analogues, while the other complex demonstrates Csp³–H bond activation proposed to occur at a Pd^I center. Overall, we consider that these studies are important since they provide strong evidence that mononuclear Pd^I species are catalytically active intermediates in cross-coupling reactions, possibly in a Pd^I/Pd^{III} catalytic cycle that is distinct from the

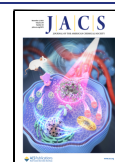
classical mononuclear Pd⁰/Pd^{II} catalysis or dinuclear Pd^I catalysis.

RESULTS AND DISCUSSION

We have previously reported the detection of a series of transient, thermally sensitive mononuclear Pd^I complexes supported by the tetradentate ligand 2,11-dithia[3.3](2,6)-pyridinophane (N2S2).³⁸ These Pd^I species were synthesized through one-electron reduction of their Pd^{II} analogues, and the soft S donor atoms of N2S2 were proposed to help stabilize the reactive Pd^I center; therefore, we continued to employ N2S2 and the related ligand 3,7-dithia-1(2,6)-pyridina-5(1,3)-benzenacyclooctaphane (NCHS2) in our efforts to isolate mononuclear Pd^I complexes. To further stabilize such Pd^I species, we considered using additional soft donor ligands such as phosphines, and we were inspired by the recent independent reports by Chaplin et al. and Ozerov et al. in isolating the [Pd^I(P^tBu₃)₂]⁺ complexes.^{39,40} We have first synthesized this Pd^I precursor and confirmed its formation via EPR spectroscopy in a glassing solvent mixture, either 1:1 1,2-difluorobenzene (DFB):2-MeTHF or 1:3 MeCN:PrCN, which also revealed superhyperfine coupling to the two ³¹P atoms in the g_z direction for both [Pd^I(P^tBu₃)₂]⁺ and

Received: August 17, 2022

Published: October 18, 2022



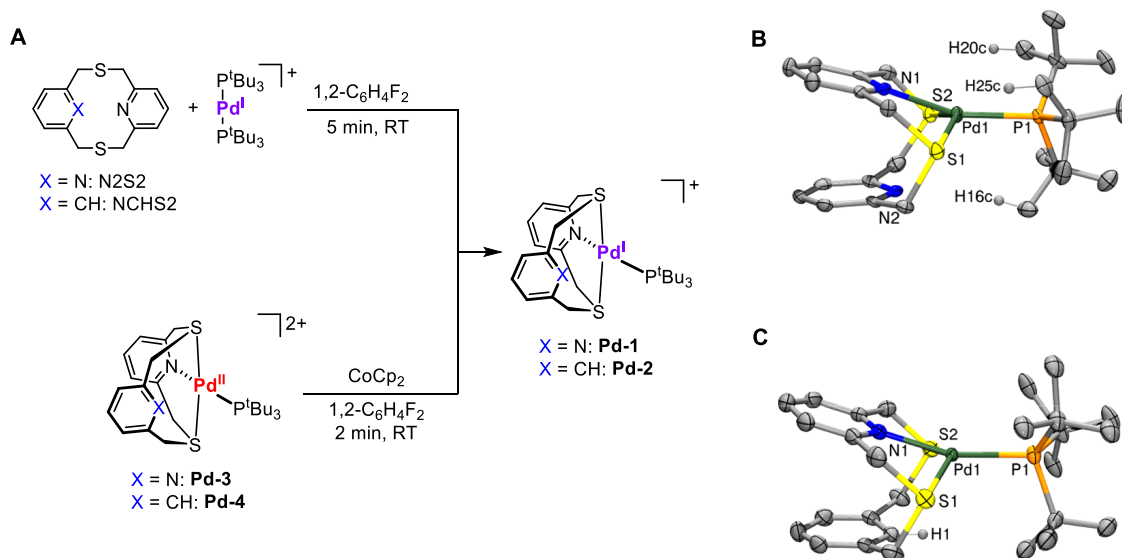


Figure 1. Synthetic routes for **Pd-1** and **Pd-2** and their X-ray crystal structures. (A) Two different pathways for the synthesis of **Pd-1** and **Pd-2**. (B) and (C) ORTEP representations (50% probability ellipsoids) of the cations of **Pd-1** (B) and **Pd-2** (C). Selected bond distances (Å) and angles (°) for **Pd-1**: Pd1–N1 2.212(5), Pd1–P1 2.3401(16), Pd1–S1 2.4775(16), Pd1–S2 2.5959(17), Pd1···H16c 2.89(7), Pd1···H20c 2.80(5), Pd1···H25c 2.98(5), Pd1···C16 3.518(7), Pd1···C20 3.474(7), Pd1···C25 3.657(7), Pd1–H16c–C16 130.0(6), Pd1–H20c–C20 124.0(4), Pd1–H25c–C25 128.0(4); and **Pd-2**: Pd1–N1 2.200(3), Pd1–P1 2.3561(13), Pd1–S1 2.5245(16), Pd–S2 2.597(2), Pd1···H1 2.61(6), Pd1···C1 3.032(4), Pd1–H1–C1 109.0(4).

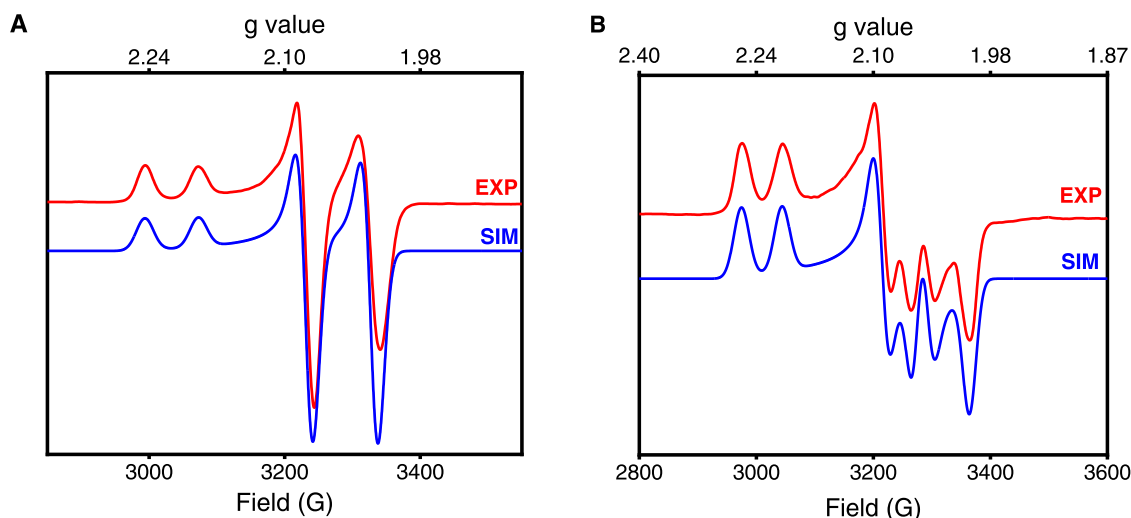
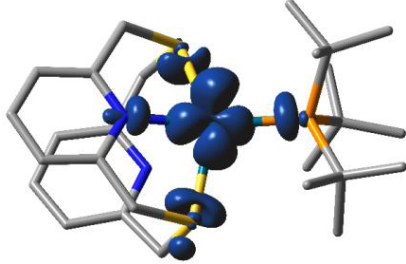
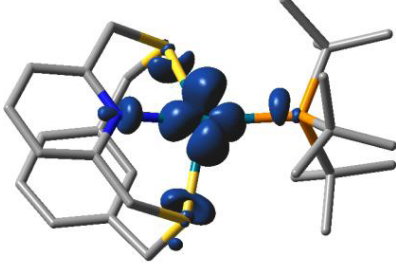


Figure 2. EPR spectra (red lines) of (A) **Pd-1** and (B) **Pd-2** in 1:1 DFB:2-MeTHF glass at 77 K, and the simulated EPR spectra (blue lines) using the following parameters: (A) $g_x = g_y = 2.050$ ($A_p = 96$ G), $g_z = 2.219$ ($A_p = 79$ G); (B) $g_x = 2.030$ ($A_p = 96$ G), $g_y = 2.070$ ($A_p = 76$ G), $g_z = 2.237$ ($A_p = 69.5$ G).

$[\text{Pd}^{\text{I}}(\text{P}^t\text{Bu}_3)_2(\text{MeCN})]^+$ complexes that was not observed previously (Figures S21 and S22).^{39,40} To our delight, two Pd^{I} complexes, $[(\text{N}2\text{S}2)\text{Pd}^{\text{I}}(\text{P}^t\text{Bu}_3)]^+$ (**Pd-1**) and $[(\text{NCHS}2)\text{Pd}^{\text{I}}(\text{P}^t\text{Bu}_3)]^+$ (**Pd-2**) were obtained upon the reaction of $[\text{Pd}^{\text{I}}(\text{P}^t\text{Bu}_3)_2]^+$ with N2S2 or NCHS2 in DFB (Figure 1A). **Pd-1** and **Pd-2** were crystallized by slow diffusion of n-pentane into DFB at -35 °C, and their single-crystal X-ray structures reveal that the Pd–P bonds of **Pd-1** and **Pd-2** are 2.3401(16) and 2.3561(13) Å, respectively (Figure 1B,C), which are comparable to the average Pd–P bond length of 2.3469(6) Å for $[\text{Pd}^{\text{I}}(\text{P}^t\text{Bu}_3)_2]^+$.^{39,40} Each Pd center is four-coordinate, with the N2S2 or NCHS2 ligand binding in a κ^3 conformation via the two S atoms and one N atom, while the P^tBu_3 ligand completes the coordination environment. Interestingly, each ^tBu group of the P^tBu_3 ligand has one methyl C–H bond

oriented toward the Pd center, with the shortest P···H–C distance of 2.80 Å (Figure 1B), and this likely plays a role in the stability of **Pd-1** and its mode of decomposition (see below). By comparison, in **Pd-2**, the shortest Pd···H–C distance of 2.61 Å is observed for the $\text{C}_{\text{ipso}}\text{-H}$ group of the phenyl ring in the NCHS2 ligand, although the rigid nature of the macrocyclic ligand likely hinders further interaction with the Pd center. Both complexes exhibit a distorted seesaw geometry, with the geometry index of $\tau'_4 = 0.161$ for **Pd-1** and $\tau'_4 = 0.166$ for **Pd-2**, respectively.⁴² In our previous study, we were able to fully characterize the Pd^{I} dinuclear complex $[(\text{N}2\text{S}2)\text{Pd}^{\text{I}}(\mu\text{-}t\text{BuNC})]_2(\text{ClO}_4)_2$,³⁸ in which the N2S2 ligand interacts with the Pd^{I} center through only one Pd–S bond. By comparison, the NXS2 ligands (X = N or CH) in the mononuclear complexes **Pd-1** and **Pd-2** have both S atoms

Table 1. DFT-Calculated Mulliken Spin Densities for Pd-1 and Pd-2 (Shown as 0.05 Isodensity Contour Plots), along with the Relevant Atomic Orbital Contributions to the Spin Density, and the Experimental and Calculated EPR Parameters

Complex	Pd-1			Pd-2		
Spin Density						
	Pd 0.646	P 0.084	2S 0.160	Pd 0.623	P 0.080	2S 0.156
	d 0.545	p 0.072	N _{eq} 0.044	d 0.555	p 0.067	N 0.042
	p 0.039	s 0.010		p 0.040	s 0.012	
	s 0.024			s 0.028		
<i>g</i> values (expt)	2.050; 2.050; 2.219			2.030; 2.070; 2.237		
<i>g</i> values (calcd)	2.046; 2.079; 2.202			2.042; 2.090; 2.216		
<i>A_p</i> values, MHz (G, expt)	269 (96); 269 (96); 222 (79)			269 (96); 213 (76); 195 (69.5)		
<i>A_p</i> values, MHz (calcd)	322; 236; 233			305; 226; 222		

bound to the Pd centers. In addition, we have synthesized the Pd^{II} complexes [(N2S2)Pd^{II}(P^tBu₃)₂]²⁺, **Pd-3**, and [(NCHS2)Pd^{II}(P^tBu₃)₂]²⁺, **Pd-4** (Figure 1A), which exhibit well-defined, reversible Pd^{II}/Pd^I redox waves at -0.47 V for **Pd-3** and -0.38 V vs Fc^{0/+} for **Pd-4**, respectively (Figures S19 and S20). As such, the Pd^I complexes **Pd-1** and **Pd-2** could also be synthesized via the one-electron reduction of **Pd-3** and **Pd-4** with CoCp₂ (Cp = cyclopentadienyl, Figure 1A), as confirmed by the EPR spectra of the reduced complexes that are identical to those of isolated **Pd-1** and **Pd-2** (see above).

Both **Pd-1** and **Pd-2** were characterized by UV–vis spectroscopy, Evans method, EPR spectroscopy, and theoretical calculations. The stability of these Pd^I complexes was investigated by UV–vis spectroscopy by monitoring the formation and decay of **Pd-1** and **Pd-2** at RT. Both **Pd-1** ($\lambda_{\text{max}} = 334$ nm, Figures S34 and S35) and **Pd-2** ($\lambda_{\text{max}} = 342$ nm, Figures S36 and S37) exhibit a slow decay of their absorption bands of <10 and <5%, respectively. Overall, the UV–vis data indicate a slower decay for **Pd-2** compared to **Pd-1**, which is likely playing a role in their reactivity profiles (see below).

Magnetic moments of $1.69 \mu_{\text{B}}$ and $1.72 \mu_{\text{B}}$ for **Pd-1** and **Pd-2**, respectively, by the Evans method at RT in DBF, suggest that these complexes have one unpaired electron. The EPR spectrum of **Pd-1** in 1:1 DFB:2-MeTHF at 77 K reveals an axial signal with $g_x = g_y = 2.050$ and $g_z = 2.219$, along with superhyperfine coupling interactions with the ³¹P atom ($I = 1:2$, 100% abundance) of 96 G and 79 G in the *x/y* and *z* directions, respectively (Figure 2A). In contrast, the EPR spectrum of **Pd-2** shows a rhombic signal with $g_x = 2.030$, $g_y = 2.070$, and $g_z = 2.237$, along with superhyperfine coupling constants of 96 G, 76 G, and 69.5 G in the *x*, *y*, and *z* directions, respectively (Figure 2B). The more anisotropic nature of the EPR spectrum of **Pd-2** than that of **Pd-1** is likely due to the presence of a phenyl group instead of a pyridyl

group in the NCHS2 ligand, which decreases the symmetry about the Pd^I center in **Pd-2**. For **Pd-1**, it is possible that in solution, a dynamic exchange between the two pyridyl N donors that can bind to the Pd center generates a pseudo-trigonal bipyramidal 5-coordinate Pd^I center and thus leads to a more axial EPR spectrum than what would be predicted based on the static X-ray structure and calculated EPR parameters (see above). The EPR experiments also indicate that these two Pd^I complexes are quite stable at low temperatures, an appreciable amount of EPR signal being observed even after storing the two Pd^I solutions at -80 °C for up to 10 days (Figures S25 and S28). Taken together, the observed structural and EPR parameters for **Pd-1** and **Pd-2** strongly suggest the presence of a d⁹ Pd^I center, with the unpaired electron being localized mainly in the d_{*x*²-*y*²} orbital.

Density functional theory (DFT) calculations further support a metal-based radical description for the Pd^I complexes **Pd-1** and **Pd-2**. The DFT-calculated spin density for **Pd-1** shows the unpaired electron resides mostly (~65%) on the Pd center—specifically in the d_{*x*²-*y*²} orbital, with appreciable contribution from the P atom (8.4%), the two S atoms (16% combined), and the equatorial N atom (4.5%, Table 1), while for **Pd-2**, the calculated spin density is localized mostly (~62%) on the Pd center, with appreciable contribution from the P atom (8%), the two S atoms (15.6% combined), and the N atom (4%, Table 1). This shows a remarkable increase in spin density on the palladium ion compared to the other recently reported heteroleptic Pd^I-amido complex, in which the SOMO only demonstrated 39.9% Pd character.⁴¹ Importantly, the appreciable contribution of the P atom to the spin density supports the observed superhyperfine coupling constants observed in all three *x*, *y*, and *z* directions, while the DFT-calculated *g* values and superhyperfine coupling constants for **Pd-1** and **Pd-2** are closely matching the experimental values (Table 1). Furthermore, the average value (*A*_{iso}) of the ³¹P

superhyperfine coupling constants and the extent of anisotropy for the A_x , A_y , and A_z values can be used to calculate the contributions of the P 3s and 3p orbitals to the spin density, respectively, following the method developed by Morton and Preston.⁴³ Using this approach and based on the experimental A_p values, it can be calculated that in **Pd-1**, the P 3s and 3p orbitals contribute 1.8 and 4.4% to the unpaired electron spin density, respectively, for a total of 6.2% contribution of the P atom to the spin density. Similarly, it was determined that in **Pd-2**, the P 3s and 3p orbitals contribute 1.7 and 6.8% to the unpaired electron spin density, respectively, for a total of 8.5% contribution of the P atom to the spin density. Overall, these experimentally derived P atom contributions to the spin density are in excellent agreement with the DFT-calculated values and strongly support the metalloradical nature of these Pd^I complexes.

Next, we sought to probe the reactivity of these Pd^I complexes in the realm of cross-coupling reactions. The commonly accepted mechanism for palladium cross-coupling reactions involves two-electron oxidative addition (OA), transmetalation, and reductive elimination (RE) steps in a Pd⁰-Pd^{II} cycle. We, however, are interested in the potential of a Pd^I-Pd^{III} cycle (Figure 3A), in which oxidative addition occurs at Pd^I to give a Pd^{III} intermediate (species **a**). To provide experimental evidence for this potential mechanism, the reaction between **Pd-2** and the aryl halides PhBr and PhI were studied by EPR. Addition of up to 10 equiv PhBr did not result in the formation of any new signals by EPR. However, upon addition of 1 equiv PhI to a solution of **Pd-2** at -45 °C, the rhombic EPR signal corresponding to **Pd-2** disappears, and a new set of features forms within minutes at -45 °C (Figure S29). The resulting EPR spectrum is stable for minutes at RT and can be simulated using a major pseudo-axial signal with $g_x = 1.999$, $g_y = 2.005$, $g_z = 2.100$ (Figure 3B) and a minor component with $g_x = g_y = 2.021$, $g_z = 2.091$ in a ~7:1 ratio (Figure 3B). However, the presence of a single species that exhibits superhyperfine coupling to the ³¹P atom of P^tBu₃ in the z-direction cannot be excluded (Figure S32). Given the proposed oxidative addition step of PhI to **Pd-2**, we tentatively assign this new EPR signal to the Pd^{III} species **a** (Figure 3A). While additional studies are needed to unambiguously confirm the nature of these species, the resulting EPR signal supports a change in the oxidation state and represents the first reported oxidative addition occurring directly at a mononuclear Pd^I center to generate a Pd^{III} species.

Having demonstrated the ability of **Pd-2** to oxidatively add to PhI, we were interested in determining the catalytic competency of the Pd^I complexes. The Kumada cross-coupling reaction between PhBr or PhI and a secondary alkyl nucleophile, cyclohexylMgCl, was employed, since these types of Csp³-Csp² cross-coupling reactions catalyzed by Pd are uncommon.^{16,44-52} PhBr showed superior yields to PhI (see below) and so PhBr was chosen as the coupling partner for reaction optimization. The **Pd-2** complex, either generated in situ or used as isolated, shows very good catalytic activity (86% by GC-FID) under mild conditions (Table 2, entries 1 and 2, respectively), and a gram-scale reaction reveals a similar yield (Figure S43). By comparison, **Pd-1** shows nearly complete ablation of the cross-coupled product under the same conditions (Table 2, entry 5). The superior reactivity of **Pd-2** relative to **Pd-1** is likely due to the additional open coordination site achieved by replacing the second pyridyl group with a phenyl group in NCHS2 vs N2S2. The Pd^{II}

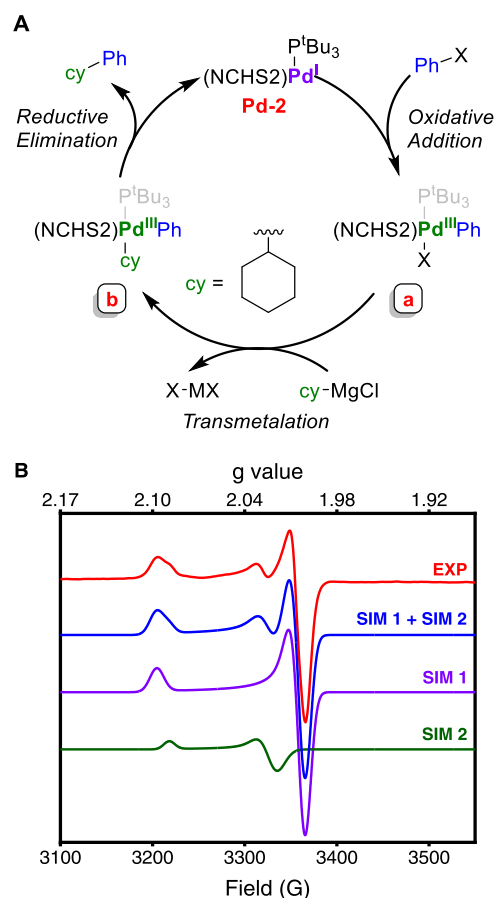
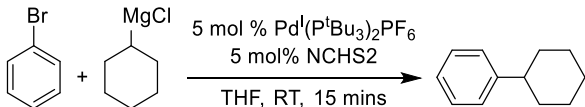


Figure 3. (A) Proposed mechanism for the Pd^I-catalyzed Kumada cross-coupling between PhI and cyclohexylMgCl (while we consider that P^tBu₃ does not bind to the Pd^{III} center due to sterics, we cannot completely exclude this possibility). (B) EPR spectrum (red line) of the resulting putative Pd^{III} species **a** formed upon the reaction of **Pd-2** with and 1 equiv PhI for 10 min at RT (spectrum collected in 1:1 DFB:2 MeTHF glass, 77 K) and the simulated EPR spectrum (blue line) using the following parameters for the species Sim 1: $g_x = 1.999$, $g_y = 2.005$, $g_z = 2.100$, and Sim 2: $g_x = g_y = 2.021$, $g_z = 2.091$ in a ~7:1 ratio.

equivalent of **Pd-2**, **Pd-4**, also shows a good reaction yield (Table 2, entry 8), though slightly lessened compared to that of its Pd^I analogue. EPR control reactions between **Pd-4** and 0.5 equiv of cyclohexylmagnesium chloride show a weak signal matching the Pd^I complex **Pd-2**, demonstrating that Grignard reagents are capable of reducing the Pd^{II} complex in situ to generate the catalytically active Pd^I complex (Figure S33). Finally, side product distribution shows that largely the β -hydride eliminated Grignard and the protodehalogenated arene account for the decrease in yield, with no starting material being observed by GC-FID after 15 min under normal conditions, and with no discernible formation of the homocoupled biphenyl product (Table S2). To the best of our knowledge, this is the first example of a Csp³-Csp² Kumada cross-coupling reaction catalyzed by isolated mononuclear Pd^I complexes that supports the direct role of Pd^I species in the Kumada cross-coupling proposed by Knochel et al. upon the generation in situ of Pd^I intermediates formed in the presence of alkyl iodides.⁴ To resolve the discrepancy between the lack of EPR reactivity with PhBr and the superior cross-coupling reactivity, we performed EPR experiments under catalytic conditions. Addition of 20 equiv cyclo-

Table 2. Optimization of the Kumada Cross-Coupling Reaction between Bromobenzene and Cyclohexylmagnesium Chloride



entry	change in conditions	yield (%) ^a
1	no change	86
2	isolated Pd-2	87
3	10 min reaction time	64
4	0 °C instead of RT	78
5	5 mol % N2S2 instead of 5 mol % NCHS2	<1
6	[Pd ⁰ (P ^t Bu ₃) ₂] instead of Pd-2	2
7	[Pd ^I (P ^t Bu ₃) ₂] ⁺ instead of Pd-2	22
8	Pd-4 instead of Pd-2	80
9	Pd(OAc) ₂ instead of Pd-2	4
10	no [Pd ^I (P ^t Bu ₃) ₂] ⁺ , NCHS2 only	0
11	no [Pd ^I (P ^t Bu ₃) ₂] ⁺ or NCHS2	0

^aYields were determined using GC-FID, with dodecane as the internal standard.

hexylmagnesium chloride to a solution of **Pd-2** and 20 equiv PhBr results in the generation of a weak EPR signal with $g_x = 1.997$, $g_y = 2.080$, and $g_z = 2.099$ (Figure S30). A similar EPR signal is observed under catalytic conditions for PhI, although additional paramagnetic signals

are present in this case, supporting our hypothesis that the less selective cross-coupling reactivity for aryl iodides is likely due to halogen exchange and the formation of additional Pd(III) species leading to side products, and as confirmed by GC-MS analysis of the EPR solution showing the formation of a significant amount of homocoupled product biphenyl (Figure S31). We also propose that the lack of an observable oxidative addition product in the presence of PhBr and the absence of the Grignard reagent may be due to the rapid equilibrium of the oxidative addition process.

After demonstrating the catalytic capability of **Pd-2**, a substrate scope containing various aryl halides with primary and secondary alkyl Grignard reagents ($R = \text{cyclohexyl}$ or $n\text{-octyl}$) was established (Tables S3 and S4). **Pd-2** demonstrated good coupling prowess with electron-rich to electron-neutral aryl bromides, with a significant decrease in yield when electron-poor arenes were used instead. Cyclohexylmagnesium chloride generated significantly higher yields of $\text{Csp}^3\text{-Csp}^2$ coupled product over $n\text{-octyl}$ magnesium chloride due to a large decrease in $\beta\text{-hydride}$ elimination across all reactions (Table S2). Additionally, aryl bromides were proven to be better coupling partners under these conditions relative to aryl iodides. Control experiments of the reactions of aryl iodides versus aryl bromides with the Grignard reagent in the absence of a catalyst show the generation of alkyl iodides but not alkyl bromides by GC-FID, suggesting magnesium–halogen exchange is operative and a contributing factor toward the

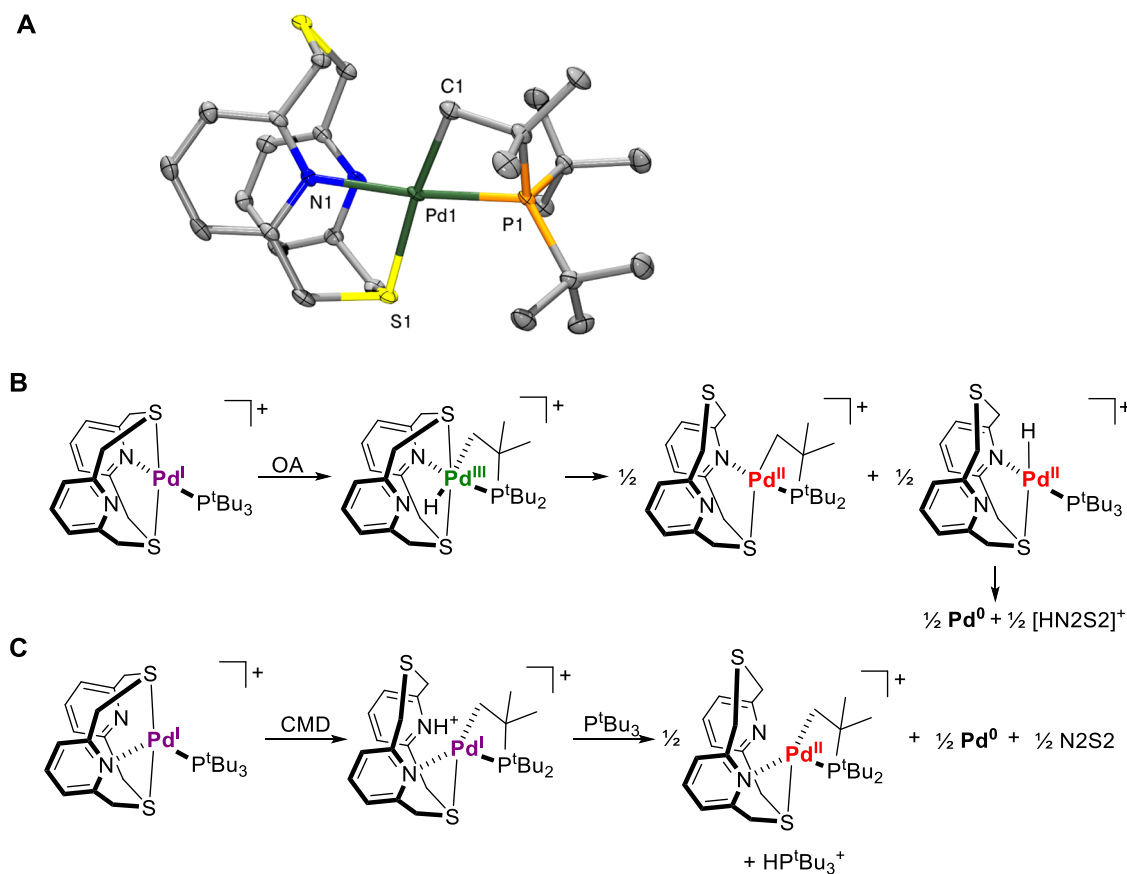


Figure 4. (A) ORTEP representation (50% probability ellipsoids) of the cation of **Pd-5**. Selected bond distances (Å) and angles (°): Pd1–C1 2.093(3), Pd1–N1 2.166(2), Pd1–P1 2.2128(8), Pd1–S1 2.3617(8), C1–Pd1–S1 168.35(8), and N1–Pd1–P1 172.12 (7). (B) Oxidative addition mechanism for the generation of **Pd-5** from **Pd-1**. (C) CMD mechanism for the generation of **Pd-5** from **Pd-1** using P^tBu₃ as the base.

decrease in yield for aryl iodides (Figure S39, middle). Additionally, the higher yields observed for *n*-octyl magnesium chloride over cyclohexylmagnesium chlorides toward aryl iodides may be explained by decreased magnesium–halogen exchange as no octyl iodide was observed by GC (Figure S39, bottom). Initial rate measurements for the reaction between PhBr and cyclohexylmagnesium chloride demonstrate a zero-order dependence on the electrophile concentration (Figure S42), and Hammett analysis for the reactions between various aryl bromides and cyclohexylmagnesium chloride shows a negative rho value ($\rho = -0.1$, Figure S40), further supporting an assignment of reductive elimination as the rate-determining step of the reaction, as the catalytic rates do not seem to depend on the ease of oxidative addition.^{53,54} Reexamination of the rho value via competition initial rate measurements shows a strongly positive value ($\rho = 3.5$, Figure S41), which supports a mechanistic proposal where oxidative addition and transmetalation is fast, resulting in a “trapped state,” which prevents the formation of the oxidative addition products from the electron-rich aryl halides despite being better suited for the overall cross-coupling reaction. Altogether, these experiments strongly support a Pd^I–Pd^{III}–Pd^{III} catalytic cycle where oxidative addition and transmetalation steps are fast, followed by a rate-limiting reductive elimination step (Figure 3A).

Interestingly, upon storing a 1:1 mixture of N2S2 and [Pd^I(P^tBu₃)₂]⁺ in MeCN at –35 °C for a few days, light yellow crystals were obtained upon layering with Et₂O. Single-crystal X-ray structural analysis of this product reveals the formation of the cyclometalated complex [(N2S2)Pd^{II}(κ_{P,C}²-P^tBu₂CMe₂CH₂)]⁺ (Pd-5), in which the Pd^{II} species adopts a distorted square planar geometry with a geometry index $\tau_4 = 0.127$ (Figure 4A).⁴² The Pd–P and Pd–C bond lengths and the P1–Pd1–C1 bite angle for the cyclometalated phosphine are comparable to the previously reported cyclometalated Pd^{II} complexes [(P^tBu₃)Pd(κ_{P,C}²-P^tBu₂CMe₂CH₂)(OAc)]HOAc⁵⁵ and [Pd(κ_{P,C}²-P^tBu₂CMe₂CH₂)(P^tBu₃)](PF₆).⁵⁶ The formation of complex Pd-5 was also confirmed by its independent synthesis and X-ray characterization from the cyclometalated Pd^{II} precursor (Figures S10, S12, and S13). Additionally, NMR of the Pd^I(P^tBu₃)₂ precursor in the presence of 1 equivalent of N2S2 generates signals corresponding to those observed for the independently synthesized cyclometalated compound (Figure S11). To the best of our knowledge, formation of Pd-5 is the first definitive characterization of an intramolecular C–H bond activation that proceeds from a mononuclear Pd^I center. In 2016, Chaplin et al. and Ozerov et al. have independently observed a similar cyclometallation process that was proposed to occur at the Pt^I center of the [Pt^I(P^tBu₃)₂]⁺ complex, yielding a mixture of Pt^{II} cyclometalated and Pt^{II}-hydride complexes.^{39,40} However, while Chaplin et al. have proposed the analogous C–H bond activation and cyclometallation to occur at the Pd^I congener [Pd^I(P^tBu₃)₂]⁺, only indirect NMR evidence from an intractable reaction mixture was provided for such a cyclometalated Pd^{II} complex. Utilizing our N2S2 ligand, we have been able to lend additional support to their hypothesis. Finally, the Pd^{II} complex Pd-3 [(N2S2)-Pd^{II}(P^tBu₃)₂]²⁺ does not undergo C–H bond activation even after 6 days at RT (Figure S3), further supporting the increased C–H bond activation reactivity of the Pd^I center in Pd-1.

The formation of the cyclometalated complex Pd-5 can be proposed to occur via one of the following mechanisms: an OA pathway (Figure 4B) or a concerted metalation–deprotonation

(CMD) pathway (Figure 4C). Both mechanisms will lead to the formation of 0.5 equiv of metallic Pd⁰, which was confirmed by the formation of a small amount of black precipitate in the reaction solution. By comparison, the formation of an analogous cyclometalated Pd^{II} complex was not observed for the NCHS2 Pd^I complex Pd-2—which is also more thermally stable, presumably due to the absence of a second pyridyl group in NCHS2, and thus it likely precludes a base-assisted CMD process.

CONCLUSIONS

In summary, we have synthesized and characterized two novel mononuclear Pd^I complexes, Pd-1 and Pd-2, stabilized by the dithiapyridinophane ligands N2S2 and NCHS2, respectively. Both complexes were fully characterized through X-ray diffraction, Evans method, UV–vis and EPR spectroscopies, and DFT calculations to confirm the formal +1 oxidation state assignment for the Pd center. Furthermore, Pd-2 is an active catalyst for the Csp²–Csp³ Kumada cross-coupling reaction, while Pd-1 exhibits a well-characterized C–H bond activation at a Pd^I center. These findings underline the importance of understanding in detail the reactivity of low-valent Pd intermediates and most importantly, highlight new potential reaction pathways for Pd catalysis in which mononuclear Pd^I species can act as the catalytically active intermediates in a range of Pd-promoted organic transformations, and thus beyond their more common use as precatalysts for classical Pd⁰/Pd^{II} catalysis.

ASSOCIATED CONTENT

Supporting Information

The Supporting Information is available free of charge at <https://pubs.acs.org/doi/10.1021/jacs.2c08765>.

Synthetic details, spectroscopic characterization, stoichiometric and catalytic reactivity studies, and crystallographic data (PDF)

Accession Codes

CCDC 2079193–2079197 contain the supplementary crystallographic data for this paper. These data can be obtained free of charge via www.ccdc.cam.ac.uk/data_request/cif, or by emailing data_request@ccdc.cam.ac.uk, or by contacting The Cambridge Crystallographic Data Centre, 12 Union Road, Cambridge CB2 1EZ, UK; fax: +44 1223 336033.

AUTHOR INFORMATION

Corresponding Author

Liviu M. Mirica – Department of Chemistry, University of Illinois at Urbana-Champaign, Urbana, Illinois 61801, United States; orcid.org/0000-0003-0584-9508; Email: mirica@illinois.edu

Authors

Giang N. Tran – Department of Chemistry, University of Illinois at Urbana-Champaign, Urbana, Illinois 61801, United States

Bailey S. Bouley – Department of Chemistry, University of Illinois at Urbana-Champaign, Urbana, Illinois 61801, United States

Complete contact information is available at: <https://pubs.acs.org/doi/10.1021/jacs.2c08765>

Author Contributions

[†]G.N.T. and B.S.B. contributed equally to this work.

Notes

The authors declare no competing financial interest.

ACKNOWLEDGMENTS

This work was supported by the National Science Foundation (CHE-2102544 to L.M.M.). The authors thank Dr. Yung-Ching Wang for his help with recording the initial EPR spectra for these studies and Prof. Nigam P. Rath (Univ. of Missouri - St. Louis) for obtaining the crystal structures of **Pd-1**, **Pd-2**, **Pd-3**, **Pd-4**, and **Pd-5**. The authors also thank all of the research facilities in the Department of Chemistry at the University of Illinois at Urbana-Champaign for their help.

REFERENCES

- (1) Hartwig, J. F. *Organotransition Metal Chemistry: From Bonding to Catalysis*; University Science Books: Sausalito, 2010.
- (2) Seechurn, C. C. C. J.; Kitching, M. O.; Colacot, T. J.; Snieckus, V. Palladium-catalyzed cross-coupling: a historical contextual perspective to the 2010 Nobel Prize. *Angew. Chem., Int. Ed.* **2012**, *51*, 5062–5085.
- (3) Gildner, P. G.; Colacot, T. J. Reactions of the 21st Century: Two Decades of Innovative Catalyst Design for Palladium-Catalyzed Cross-Couplings. *Organometallics* **2015**, *34*, 5497–5508.
- (4) Manolikakes, G.; Knochel, P. Radical catalysis of Kumada cross-coupling reactions using functionalized Grignard reagents. *Angew. Chem., Int. Ed.* **2009**, *48*, 205–209.
- (5) Liu, Q.; Dong, X.; Li, J.; Xiao, J.; Dong, Y.; Liu, H. Recent Advances on Palladium Radical Involved Reactions. *ACS Catal.* **2015**, *5*, 6111–6137.
- (6) Parasram, M.; Chuentragool, P.; Sarkar, D.; Gevorgyan, V. Photoinduced Formation of Hybrid Aryl Pd-Radical Species Capable of 1,5-HAT: Selective Catalytic Oxidation of Silyl Ethers into Silyl Enol Ethers. *J. Am. Chem. Soc.* **2016**, *138*, 6340–6343.
- (7) Simpson, Q.; Sinclair, M. J. G.; Lupton, D. W.; Chaplin, A. B.; Hooper, J. F. Oxidative Cross-Coupling of Boron and Antimony Nucleophiles via Palladium(I). *Org. Lett.* **2018**, *20*, 5537–5540.
- (8) Chen, X. Y.; Pu, M. P.; Cheng, H. G.; Sperger, T.; Schoenebeck, F. Arylation of Axially Chiral Phosphorothioate Salts by Dinuclear Pd-I Catalysis. *Angew. Chem., Int. Ed.* **2019**, *58*, 11395–11399.
- (9) Torres, G. M.; Liu, Y.; Arndtsen, B. A. A dual light-driven palladium catalyst: Breaking the barriers in carbonylation reactions. *Science* **2020**, *368*, 318–323.
- (10) Zhao, B.; Shang, R.; Wang, G.-Z.; Wang, S.; Chen, H.; Fu, Y. Palladium-Catalyzed Dual Ligand-Enabled Alkylation of Silyl Enol Ether and Enamide under Irradiation: Scope, Mechanism, and Theoretical Elucidation of Hybrid Alkyl Pd(I)-Radical Species. *ACS Catal.* **2020**, *10*, 1334–1343.
- (11) Colacot, T. J. A highly active palladium(I) dimer for pharmaceutical applications - [Pd(Ī1/4-Br)(tBu3P)]₂ as a practical cross-coupling catalyst. *Platinum Met. Rev.* **2009**, *53*, No. 183.
- (12) Bonney, K. J.; Proutiere, F.; Schoenebeck, F. Dinuclear Pd(I) complexes-solely precatalysts? Demonstration of direct reactivity of a Pd(I) dimer with an aryl iodide. *Chem. Sci.* **2013**, *4*, 4434–4439.
- (13) Johansson Seechurn, C. C. C.; Sperger, T.; Scrase, T. G.; Schoenebeck, F.; Colacot, T. J. Understanding the Unusual Reduction Mechanism of Pd(II) to Pd(I): Uncovering Hidden Species and Implications in Catalytic Cross-Coupling Reactions. *J. Am. Chem. Soc.* **2017**, *139*, 5194–5200.
- (14) Hazari, N.; Hruszkewycz, D. P. Dinuclear Pd(I) complexes with bridging allyl and related ligands. *Chem. Soc. Rev.* **2016**, *45*, 2871–2899.
- (15) Hazari, N.; Melvin, P. R.; Beromi, M. M. Well-defined nickel and palladium precatalysts for cross-coupling. *Nat. Rev. Chem.* **2017**, *1*, No. 0025.
- (16) Fricke, C.; Sperger, T.; Mendel, M.; Schoenebeck, F. Catalysis with Palladium(I) Dimers. *Angew. Chem., Int. Ed.* **2021**, *60*, 3355–3366.
- (17) Shaughnessy, K. H. Development of Palladium Precatalysts that Efficiently Generate LPd(0) Active Species. *Isr. J. Chem.* **2020**, *60*, 180–194.
- (18) Aufiero, M.; Scattolin, T.; Proutiere, F.; Schoenebeck, F. Air-Stable Dinuclear Iodine-Bridged Pd(I) Complex - Catalyst, Precursor, or Parasite? The Additive Decides. Systematic Nucleophile-Activity Study and Application as Precatalyst in Cross-Coupling. *Organometallics* **2015**, *34*, 5191–5195.
- (19) Christmann, U.; Pantazis, D. A.; Benet-Buchholz, J.; McGrady, J. E.; Maseras, F.; Vilar, R. Experimental and theoretical investigations of new dinuclear palladium complexes as precatalysts for the amination of aryl chlorides. *J. Am. Chem. Soc.* **2006**, *128*, 6376–6390.
- (20) Christmann, U.; Vilar, R.; White, A. J. P.; Williams, D. J. Synthesis of two novel dinuclear palladium(I) complexes and studies of their catalytic activity in amination reactions. *Chem. Commun.* **2004**, *0*, 1294–1295.
- (21) Kundu, G.; Sperger, T.; Rissanen, K.; Schoenebeck, F. A Next-Generation Air-Stable Palladium(I) Dimer Enables Olefin Migration and Selective C-C Coupling in Air. *Angew. Chem., Int. Ed.* **2020**, *59*, 21930–21934.
- (22) Pirkl, N.; Del Grosso, A.; Mallick, B.; Doppiu, A.; Goossen, L. J. Dihalogen-bridged NHC-palladium(i) dimers: synthesis, characterisation and applications in cross-coupling reactions. *Chem. Commun.* **2019**, *55*, 5275–5278.
- (23) Barder, T. E. Synthesis, structural, and electron topographical analyses of a dialkylbiaryl phosphine/arene-ligated palladium(I) dimer: Enhanced reactivity in Suzuki-Miyaura coupling reactions. *J. Am. Chem. Soc.* **2006**, *128*, 898–904.
- (24) Montgomery, M.; O'Brien, H. M.; Mendez-Galvez, C.; Bromfield, C. R.; Roberts, J. P. M.; Winnicka, A. M.; Horner, A.; Elorriaga, D.; Sparkes, H. A.; Bedford, R. B. The surprisingly facile formation of Pd(i)-phosphido complexes from ortho-biphenylphosphines and palladium acetate. *Dalton Trans.* **2019**, *48*, 3539–3542.
- (25) Vilar, R.; Mingos, D. M. P.; Cardin, C. J. Synthesis and structural characterization of [Pd₂(m-Br)₂(PBut₃)₂], an example of a palladium(I)-palladium(I) dimer. *Dalton Trans.* **1996**, *0*, 4313–4314.
- (26) Fafard, C. M.; Adhikari, D.; Foxman, B. M.; Mendiola, D. J.; Ozerov, O. V. Addition of Ammonia, Water, and Dihydrogen Across a Single Pd-Pd Bond. *J. Am. Chem. Soc.* **2007**, *129*, 10318–10319.
- (27) Huacuja, R.; Graham, D. J.; Fafard, C. M.; Chen, C.-H.; Foxman, B. M.; Herbert, D. E.; Alliger, G.; Thomas, C. M.; Ozerov, O. V. Reactivity of a Pd(I)-Pd(I) Dimer with O₂: Monohapto Pd Superoxide and Dipalladium Peroxide in Equilibrium. *J. Am. Chem. Soc.* **2011**, *133*, 3820–3823.
- (28) Jaworski, J. N.; McCann, S. D.; Guzei, I. A.; Stahl, S. S. Detection of Palladium(I) in Aerobic Oxidation Catalysis. *Angew. Chem., Int. Ed.* **2017**, *56*, 3605–3610.
- (29) Hill, L. L.; Crowell, J. L.; Tutwiler, S. L.; Massie, N. L.; Hines, C. C.; Griffin, S. T.; Rogers, R. D.; Shaughnessy, K. H.; Grasa, G. A.; Seechurn, C. C. C. J.; Li, H. B.; Colacot, T. J.; Chou, J.; Woltermann, C. J. Synthesis and X-ray Structure Determination of Highly Active Pd(II), Pd(I), and Pd(0) Complexes of Di(tert-butyl)-neopentylphosphine (DTBNpP) in the Arylation of Amines and Ketones. *J. Org. Chem.* **2010**, *75*, 6477–6488.
- (30) Hueffel, J. A.; Sperger, T.; Funes-Ardoiz, I.; Ward, J. S.; Rissanen, K.; Schoenebeck, F. Accelerated dinuclear palladium catalyst identification through unsupervised machine learning. *Science* **2021**, *374*, 1134–1140.
- (31) Fujiwara, S.; Nakamura, M. Electron Spin Resonance of Pd(I). 2. Gamma-Irradiated Single Crystals of K₂pdCl₄ and (NH₄)₂pdCl₄. *J. Chem. Phys.* **1971**, *54*, No. 3378.
- (32) Nakamura, M.; Fujiwara, S. Electron Spin Resonance of Pd(I). III: The Nature of the Metal-ligand Bonds in Square Planar Complexes of Palladium(I). *J. Coord. Chem.* **1972**, *1*, 221–227.
- (33) Broadley, K.; Lane, G. A.; Connelly, N. G.; Geiger, W. E. Electrochemical routes to paramagnetic dinuclear and mononuclear

palladium π complexes stabilized by the pentaphenylcyclopentadienyl ligand. *J. Am. Chem. Soc.* **1983**, *105*, 2486–2487.

(34) Lane, G. A.; Geiger, W. E.; Connelly, N. G. Palladium(I)- π -radicals. Electrochemical preparation and study of their reaction pathways. *J. Am. Chem. Soc.* **1987**, *109*, 402–407.

(35) Blake, A. J.; Gould, R. O.; Hyde, T. I.; Schröder, M. Stabilization of monovalent palladium by tetraaza macrocycles. *J. Chem. Soc., Chem. Commun.* **1987**, *0*, 431–433.

(36) Blake, A. J.; Gould, R. O.; Hyde, T. I.; Schröder, M. Tetrahedral Distortion in Palladium(II) Macrocyclic Complexes: The Single Crystal X-Ray Structure of $[\text{Pd}(\text{tbc})](\text{PF}_6)_2 \cdot 0.4\text{MeNO}_2$ (tbc = 1,4,8,11-tetrabenzyl-1,4,8,11-tetra-azacyclotetradecane). *J. Chem. Soc., Chem. Commun.* **1987**, *0*, 1731–1732.

(37) Reid, G.; Blake, A. J.; Hyde, T. I.; Schröder, M. Stereochemical and redox properties of palladium complexes of 1,4,10,13-tetrathia-7,16-diazacyclooctadecane. *J. Chem. Soc., Chem. Commun.* **1988**, *0*, 1397–1399.

(38) Luo, J.; Tran, G. N.; Rath, N. P.; Mirica, L. M. Detection and Characterization of Mononuclear Pd(I) Complexes Supported by N2S2 and N4 Tetradentate Ligands. *Inorg. Chem.* **2020**, *59*, 15659–15669.

(39) Troadec, T.; Tan, S. Y.; Wedge, C. J.; Rourke, J. P.; Unwin, P. R.; Chaplin, A. B. One-Electron Oxidation of $[\text{M}((\text{PBu}_3)\text{-Bu-t})(2)]$ (M=Pd, Pt): Isolation of Monomeric $[\text{Pd}((\text{PBu}_3)\text{-Bu-t})(2)]^+$ and Redox-Promoted C-H Bond Cyclometalation. *Angew. Chem., Int. Ed.* **2016**, *55*, 3754–3757.

(40) MacInnis, M. C.; DeMott, J. C.; Zolnhofer, E. M.; Zhou, J.; Meyer, K.; Hughes, R. P.; Ozerov, O. V. Cationic Two-Coordinate Complexes of Pd(I) and Pt(I) Have Longer Metal-Ligand Bonds Than Their Neutral Counterparts. *Chem* **2016**, *1*, 902–920.

(41) Liu, J.; Bollmeyer, M. M.; Kim, Y.; Xiao, D.; MacMillan, S. N.; Chen, Q.; Leng, X.; Kim, S. H.; Zhao, L.; Lancaster, K. M.; Deng, L. An Isolable Mononuclear Palladium(I) Amido Complex. *J. Am. Chem. Soc.* **2021**, *143*, 10751–10759.

(42) Okuniewski, A.; Rosiak, D.; Chojnacki, J.; Becker, B. Coordination polymers and molecular structures among complexes of mercury(II) halides with selected 1-benzoylthioureas. *Polyhedron* **2015**, *90*, 47–57.

(43) Morton, J. R.; Preston, K. F. Atomic parameters for paramagnetic resonance data. *J. Mag. Res.* **1978**, *30*, 577–582.

(44) Kalvet, I.; Sperger, T.; Scattolin, T.; Magnin, G.; Schoenebeck, F. Palladium(I) Dimer Enabled Extremely Rapid and Chemoselective Alkylation of Aryl Bromides over Triflates and Chlorides in Air. *Angew. Chem., Int. Ed.* **2017**, *56*, 7078–7082.

(45) Lehmann, J. W.; Crouch, I. T.; Blair, D. J.; Trobe, M.; Wang, P.; Li, J.; Burke, M. D. Axial shielding of Pd(II) complexes enables perfect stereoretention in Suzuki-Miyaura cross-coupling of Csp³ boronic acids. *Nat. Commun.* **2019**, *10*, No. 1263.

(46) Ma, X.; Murray, B.; Biscoe, M. R. Stereoselectivity in Pd-catalyzed cross-coupling reactions of enantioenriched nucleophiles. *Nat. Rev. Chem.* **2020**, *4*, 584–599.

(47) Blair, D. J.; Chitti, S.; Trobe, M.; Kostyra, D. M.; Haley, H. M. S.; Hansen, R. L.; Ballmer, S. G.; Woods, T. J.; Wang, W.; Mubayi, V.; Schmidt, M. J.; Pipal, R. W.; Morehouse, G. F.; Palazzolo Ray, A. M. E.; Gray, D. L.; Gill, A. L.; Burke, M. D. Automated iterative Csp³-C bond formation. *Nature* **2022**, *604*, 92–97.

(48) Xu, G. L.; Gao, P.; Colacot, T. J. Tunable Unsymmetrical Ferrocene Ligands Bearing a Bulky Di-1-adamantylphosphino Motif for Many Kinds of C-sp²-C-sp³ Couplings. *ACS Catal.* **2022**, *12*, 5123–5135.

(49) Limmert, M. E.; Roy, A. H.; Hartwig, J. F. Kumada coupling of aryl and vinyl tosylates under mild conditions. *J. Org. Chem.* **2005**, *70*, 9364–9370.

(50) Shu, C. T.; Sidhu, K.; Zhang, L.; Wang, X. J.; Krishnamurthy, D.; Senanayake, C. H. Palladium-Catalyzed Cross-Coupling of Cyclopropylmagnesium Bromide with Aryl Bromides Mediated by Zinc Halide Additives. *J. Org. Chem.* **2010**, *75*, 6677–6680.

(51) Xu, M. Y.; Jiang, W. T.; Li, Y.; Xu, Q. H.; Zhou, Q. L.; Yang, S.; Xiao, B. Alkyl Carbagermatranes Enable Practical Palladium-

Catalyzed sp²-sp³ Cross-Coupling. *J. Am. Chem. Soc.* **2019**, *141*, 7582–7588.

(52) Hayashi, T.; Konishi, M.; Kobori, Y.; Kumada, M.; Higuchi, T.; Hirotsu, K. Dichloro[1,1'-Bis(Diphenylphosphino)Ferrocene]-Palladium(II) - an Effective Catalyst for Cross-Coupling of Secondary and Primary Alkyl Grignard and Alkylzinc Reagents with Organic Halides. *J. Am. Chem. Soc.* **1984**, *106*, 158–163.

(53) Portnoy, M.; Milstein, D. Mechanism of Aryl Chloride Oxidative Addition to Chelated Palladium(0) Complexes. *Organometallics* **1993**, *12*, 1665–1673.

(54) Shekhar, S.; Hartwig, J. F. Distinct electronic effects on reductive eliminations of symmetrical and unsymmetrical bis-aryl platinum complexes. *J. Am. Chem. Soc.* **2004**, *126*, 13016–13027.

(55) Henderson, W. H.; Alvarez, J. M.; Eichman, C. C.; Stambuli, J. P. Characterization, Reactivity, and Potential Catalytic Intermediacy of a Cyclometalated Tri-tert-butylphosphine Palladium Acetate Complex. *Organometallics* **2011**, *30*, 5038–5044.

(56) Sinclair, M. J. G.; Chaplin, A. B. Oxidative ring expansion of a low-coordinate palladacycle: Synthesis of a robust T-shaped alkylpalladium(II) complex. *Inorg. Chim. Acta* **2020**, *513*, No. 119948.

Recommended by ACS

Protodemetalation of (Bipyridyl)Ni(II)-Aryl Complexes Shows Evidence for Five-, Six-, and Seven-Membered Cyclic Pathways

Paige E. Piszal, Daniel J. Weix, *et al.*

APRIL 07, 2023

JOURNAL OF THE AMERICAN CHEMICAL SOCIETY

READ 

Overview of the Synthesis and Catalytic Reactivity of Transition Metal Complexes Based on C=P Bond Systems

Aleksandra Ziólkowska, Łukasz Ponikiewski, *et al.*

MARCH 20, 2023

ORGANOMETALLICS

READ 

Stereochemistry of the Reactions between Palladacycle Complexes and Primary Alkyl Iodides

Xinyu Xu and Lei Jiao

MARCH 18, 2023

ORGANOMETALLICS

READ 

Pd(II) Complexes of Chiral Proline-Derived Ligands: Application for Dynamic Thermodynamic Resolution of α -Amino Acids and Their Antibacterial Activities

Huajian Zhu, Hong Liu, *et al.*

MARCH 03, 2023

THE JOURNAL OF ORGANIC CHEMISTRY

READ 

Get More Suggestions >